Materials Transactions, Vol. 46, No. 7 (2005) pp. 1610 to 1617
Special Issue on Medical, Healthcare, Sport and Leisure Materials

Osteocompatibility of Stainless Steel, Co–Cr–Mo, Ti–6Al–4V and Ti–15Zr–4Nb–4Ta Alloy Implants in Rat Bone Tissue

Yoshimitsu Okazaki[1], Emiko Gotoh[2], Miki Nishimori[3], Shin-ichi Katsuda[3], Takeshi Manabe[4] and Kihei Kobayashi[4]

[1]*Institute for Human Science and Biomedical Engineering, National Institute of Advanced Industrial Science and Technology, Tsukuba 305-8564, Japan*
[2]*National Institute of Technology and Evaluation, Tsukuba 305-0044, Japan*
[3]*Japan Food Research Laboratory, Tokyo 206-0025, Japan*
[4]*Nihon University of Dentistry at Matsudo, Matsudo 271-8587, Japan*

To examine the formation of a new bone using various metal implants, 316L stainless steel, Co–Cr–Mo casting alloy, and Ti–6Al–4V and Ti–15Zr–4Nb–4Ta alloys were implanted into the rat femur and tibia for up to 48 weeks. Morphometrical parameters, namely, new bone formation rate, bone contact rate, new bone thickness and osteoid formation rate were investigated. Although a thin osteoid layer in a new bone-metal interface was observed in all the alloy implants, a new bone was well formed around all the alloy implants in the bone marrow of the rat femur and tibia up to 48 weeks. Neither the resorption of bone nor inflammatory reactions such as the presence of foreign-body giant cells and infiltration of inflammatory cells were also evident in the histological examination of these implants. A normal bone remodeling was observed in the new bone-metal implant interface, and osteoblasts capable of differentiating into a new bone tissue were lined on the implant side in the new bone-metal implant interface. Many osteocytes were observed in the lamellar bone tissue. The new bone formed around all the alloy implants developed into a calcified bone consisting of lamellar structure with increasing implantation period. A capsulated fibrous connective tissue was observed in the 316L stainless steel and Co–Cr–Mo alloy implants at 48 weeks after long-term implantation. Many osteoclasts were observed at the interface between the fibrous connective tissue and lamellar bone tissue. The bone formation rates around all the alloy implants were markedly high, approximately more than 90% at 4 weeks after implantation, and thereafter, no marked change was observed. The bone contact rate of Co–Cr–Mo alloy implant was slightly higher than that of 316L stainless steel implant. In the early stage of implantation (4–12 weeks), the bone contact rates of Ti alloy implants were significantly higher than that of Co–Cr–Mo alloy implant. In the late stage of implantation (24–48 weeks), the osteoid formation rates of Co–Cr–Mo and Ti–6Al–4V alloy implants tended to increase, but not significantly. Significant differences in the bone morphometrical parameters, suggesting osteocompatibility, were detected, although histological findings were not evident. Histological examinations of undecalcified sections were essential for confirming the interface between a newly formed bone and a metal implant, and morphometrical parameters, suggested to be good markers of osteocompatibility for the investigation of various metal implants.

(Received January 20, 2005; Accepted March 11, 2005; Published July 15, 2005)

Keywords: *In vivo test, rat implantation, stainless steel, cobalt alloy, titanium alloy, osteocompatibility, morphometrical parameters, bone formation, bone contact rate, new bone thickness, osteoid formation rate*

1. Introduction

Stainless steel, Co–Cr–Mo alloy and Ti alloy have been widely used in medical implants. Osteocompatibility, osteoconduction and osteoinduction are essential properties of metal implants used as artificial joints and artificial tooth roots. Over the last few decades, the osteocompatibility of the metal implants has been the subject of controversy.[1–5] However, there is still room for further investigation involving histological analysis and histomorphometrical parameters for osteocompatibility.[1–5] The purpose of this study is to histologically examine the formation of a new bone and morphometrical parameters of osteocompatibility for various metal implants. 316L stainless steel, Co–Cr–Mo casting alloy, and Ti–6Al–4V and Ti–15Zr–4Nb–4Ta alloys were implanted into the rat femur and tibia for up to 48 weeks. The new bone formation rate, bone contact rate, new bone thickness and osteiod formation rate were measured using undecalcified bone sections. In addition to the histological examination, quantitative analyses were performed to compare the properties of various alloy implants.

2. Experimental Methods

2.1 Alloy specimens

316L stainless steel, which is used for the manufacture of surgical implants in Japan, specified in Japanese Industrial Standard (JIS) G 4303 was prepared by vacuum-induction melting. After soaking at 1200°C for 3 h, the ingot was forged. The billet soaked at 1200°C for 1 h was hot-worked. After maintaining at 1050°C for 30 min, the plate was quenched in water. Finally, the stainless steel plate was solution-treated at 1050°C for 2 min, and then quenched in water. The Co–Cr–Mo alloy specified in ISO 5832-4 was subjected to vacuum-induction melting, and then vacuum-cast by pouring at 1420°C into a mold manufactured using a lost wax process. The ingot was homogenized at 1220°C for 4 h. The Co–Cr–Mo alloy was used as a cast in an *in vivo* test. The Ti–6Al–4V extra low interstitial (ELI) alloy (ISO 5832-3) and the Ti–15Zr–4Nb–4Ta alloy specified for surgical implants in JIS T 7401-4 were subjected to vacuum-arc melting. After β (after soaking: 1150°C–3 h for Ti–6Al–4V and 1050°C–4 h for Ti–15Zr–4Nb–4Ta) and α–β forging (starting temperatures: 930°C for Ti–6Al–4V and 750°C for Ti–15Zr–4Nb–4Ta), the Ti alloys were annealed for 2 h at 700°C. The chemical compositions of stainless steel and Co–Cr–Mo and Ti alloys are shown in Table 1.

2.2 Rat implantation and preparation of undecalcified or decalcified section

Implant specimens, 1.2 mm in diameter and 2 mm in length, were cut from the alloy specimens. The edges of the column were then chamfered (C 0.1). The means and standard deviations of surface roughness (Ra) for 316L

Table 1 Chemical composition (mass %) of materials used.

	Cr	Ni	Mo	Mn	C	Si	P	S	Fe	Co
316L stainless steel	17.00	12.15	2.04	1.40	0.024	0.82	0.034	0.008	Bal.	—
Co–Cr–Mo alloy	28.36	0.3	6.1	0.42	0.27	0.63	—	—	0.46	Bal.

Titanium alloys	Zr	Nb	Ta	Pd	Fe	O	N	H	C	Al	V	Ti
Ti–15Zr–4Nb–4Ta	15.24	3.90	3.92	0.22	0.022	0.162	0.048	0.011	0.002	—	—	Bal.
Ti–6Al–4V ELI	—	—	—	—	0.179	0.174	0.0032	—	0.007	6.24	4.19	Bal.

stainless steel, Co–Cr–Mo, Ti–6Al–4V and Ti–15Zr–4Nb–4Ta alloy implant specimens were 0.11 ± 0.03, 1.32 ± 0.42, 1.36 ± 0.18, and 0.77 ± 0.07, respectively. The surface roughness was measured at two sites of the three specimens for each alloy implant.

The implantation test was also performed in reference to ISO 10993-6 (Biological evaluation of medical devices-part 6: Test for local effects after implantation). In this study, implantation tests were performed at two laboratories, namely, the Nihon University School of Dentistry at Matsudo and the Japan Food Research Laboratory.

The experimental protocol was approved by the Laboratory Animal Ethics Committee of the Nihon University School of Dentistry at Matsudo. Six-week-old male Wistar rats (purchased from Sankyo Labo Service) weighing 184 ± 30 g after more than 1 week of feeding were selected because it is at this growth period where bone formation is promoted around an implant. After pentobarbital sodium solution was intra-abdominally injected at a dose of 25 mg/kg, two sites 20 mm below the knee joints on the right and left sides were shaved, sterilized and incised using a scalpel to expose the surface of tibia and exfoliate the periosteum. For the implant cavity, two holes 1.2 mm in diameter were formed at 8 and 15 mm positions below the knee joints with an infusion of sterile physiological saline solution. Round dental burrs 0.6 and 1.2 mm in diameter rotating at a speed of 160 rpm were used, powered by a micromotor for implant surgery. Two implants of the same alloy in a limb were anteroposterior-bicortically inserted and not positioned inside the medullary cavity parallel to the longitudinal axis of the tibia. The four alloys were divided into two groups, namely, the Ti alloy (Ti–6Al–4V and Ti–15Zr–4Nb–4Ta) group and the other alloy (316L and Co–Cr–Mo) group. Different alloys of the same group were implanted separately into the left or right tibia. The incised skin was closed by mattress suture using a surgical silk suture needle. At three days after implantation, the rats were given an antibiotic. The rats' conditions were checked everyday up to the first 2 weeks after the operation and then once every 3 days thereafter. Five Wistar rats for each implantation period per group (total: 40 rats) were used. A radiograph of the rat tibia with the Ti–15Zr–4Nb–4Ta alloy implant at 12 weeks after implantation is shown in Fig. 1.

The left and right tibiae were removed at 6, 12, 24, and 48 weeks after implantation. The bones were fully washed in a physiological saline solution. The bone tissue was fixed in a 10% neutral phosphate-buffered formalin solution for more than two weeks. The procedures for the preparation of the undecalcified and decalcified bone tissue sections are shown

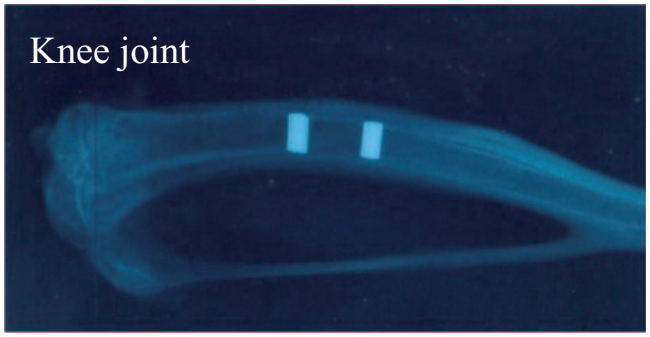

Fig. 1 Radiograph of Ti–15Zr–4Nb–4Ta alloy implant at 12 weeks after implantation.

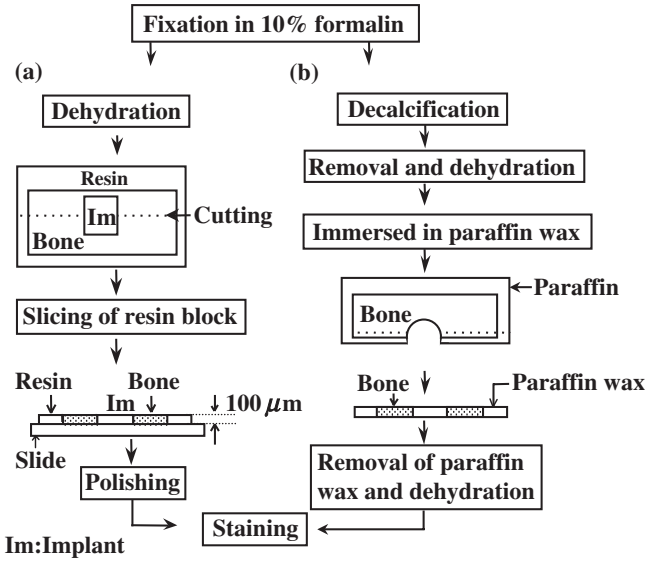

Fig. 2 Schematic diagram of preparation of microscopic sections. (a) Undecalcified section, (b) decalcified section.

in Fig. 2. In the undecalcified bone section [Fig. 2(a)], the bone tissue was dehydrated and defatted with ethanol (70%, 80% and 90% overnight, and 100% for 4 d at room temperature), xylene (for 3 d at room temperature) and 100% acetone (for 3 d at room temperature) successively. The bone tissue was then immersed in resin (0steobet I and 0steobet II) for 7 d at 4°C, and embedded in fresh resin (0steobet) for 3 d at 35°C successively. The bone tissues embedded in the resin were crosscut using a diamond blade (Microtom, SP1600, Lieca Co., Ltd.) to a thickness of approximately 100 μm at the longitudinal center of the metal implant, the position approximately 300 μm upward from the center, and the position approximately 300 μm downward

Table 2 Relationship between various stains and dyed finishes.

Stains	Subject	Connective tissue	Osteoid	Calcified bone	Nuclear
Villanueva	Bright field		Reddish purple	Colorless~ Light brown	Reddish purple
	Fluorescence		Red	Yellowish green~ green	Red
Giemsa			Blue	Light blue	Reddish purple
Toluidine blue			Blue	Light blue	Blue
Hematoxylin and eosin		Light red	Red	Purple	
Azan-Malloy		Blue		Red	Dark red

from the center (transverse sectioning). The sliced resin block was then polished to a thickness below 40 μm using waterproof emery paper from #600 to #4000 grit, followed by staining using toluidine blue (TB) and Villanueva stains. The decalcified bone section was used to observe the bone tissue reactions at a high amplification rate. For decalcified bone sectioning [Fig. 2(b)], after fixation, another bone tissue was decalcified using a 5% formalin solution containing 5% formic acid (pH = 2.3, 10% formalin: 10% formic acid = 1:1) at 4°C for 3 d. After decalcifying, the bones were neutralized in a 5% aqueous sodium sulfate solution for 24 h, and then washed in running water for 24 h. Thereafter, the bone tissue was carefully cut using a blade parallel to the length of the tibia, so as to divide the implant into two sections along its vertical axis. Then, the implant was removed. The bone tissue was dehydrated and defatted with ethanol (70, 70, 90, 100, 100 and 100% for 1 h at room temperature) and xylene (I, II and III for 1 h at room temperature) successively. The bone tissue was immersed in paraffin wax (I, II and III for 1 h at room temperature) successively. The bone tissue containing the penetrated paraffin wax was placed in a cooled metallic mold and the melted fresh paraffin wax was then poured into it. The specimens embedded in the paraffin wax were sliced to a thickness of approximately 4 μm using a microcutting machine. More than twenty slices were obtained from the center part of the vertical axis of the metal implant. After removing the paraffin wax and dehydration, these sliced sections were stained using hematoxylin eosin (HE) and Azan-Malloy (AM) stains to observe bone remodeling and connective tissues. The bone tissues newly formed around the metal implant were histologically examined using an optical micrograph.

In an animal implantation test at the Japan Food Research Laboratory, Co–Cr–Mo, Ti–6Al–4V and Ti–15Zr–4Nb–4Ta alloys were implanted. After five weeks of feeding, male Wister/ST rats (purchased from Japan SLC, Inc.) were used at 15 weeks of age (weight: 380 ± 14 g). The animals were anesthetized with sodium pentobarbital at a dose of 40 mg/kg, and the femur and tibia on the right and left sides were shaved, sterilized and incised using a scalpel. A hole with a diameter of 1.2 mm was made in the right femur using an electric trimmer, and an alloy was inserted into the hole. In the left femur and both tibiae, the same alloy was implanted in the same manner. At the end of each implantation period (4, 12, 24 and 48 weeks), the animals were sacrificed under general anesthesia. Three to five Wistar rats for each implantation period per alloy specimen (total: 48 rats) were used. Bones including metal implants were excised and fixed in formalin, dehydrated in ethanol and acetone, and embedded in polyester resin. The bone tissues embedded in the resin were sliced using a diamond blade parallel to the length of the femur or tibia, so as to divide the metal implant into two sections along its vertical axis (vertical sectioning). The sliced resin section was then polished to approximately 70 to 80 μm using an electric file, followed by staining using the Villanueva stain to discriminate the osteoid from the calcified bone. The toluijine blue and Giemsa stains were used for the histologial analysis of the bone tissue. The osteoid formation rate was measured under a fluorescent microscope using specimens subjected to Villanueva staining. The relationship between various stains and dyed finishes is summarized in Table 2. The body weight of the rats used in this study linearly increased up to 24 weeks, but negligibly increased at 48 weeks after implantation, as shown in Fig. 3.

2.3 Morphometry

A schematic illustration for estimating the morphometrical parameters of the new bone in the transverse and vertical undecalcified bone sections is shown in Fig. 4. The new bone tissues that formed around the surface of the metal implant were compared using the following four parameters: (1) new bone formation rate (%) = (total length of new bone formed around implant)/(surrounding length of implant existing in bone marrow) × 100; (2) bone contact rate (%) = (total length in direct contact with implant)/(surrounding length of implant in bone marrow) × 100; (3) osteoid formation rate (%) using the Villanueva stain = [(total area of osteoid)/total area of new bone (osteoid plus calcified bone)] × 100; and (4) new bone thickness = (total area of new bone)/(total length of new bone formed around metal implant). The new bone thickness in the vertical section [Fig. 4(b)] was calculated using the following formula: [length of new bone minus root of {(length of new bone)^2 minus 16(area of new bone)}]/4. These parameters were measured in the bone sections under a microscope with an image analysis system

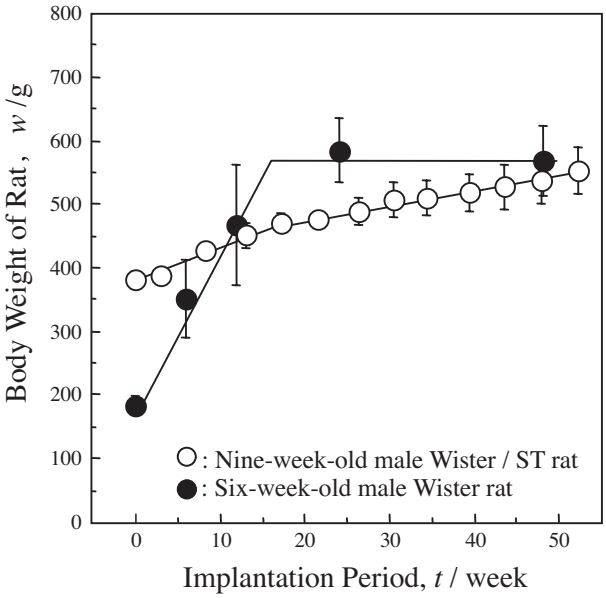

Fig. 3 Changes in body weight after implantation in rat.

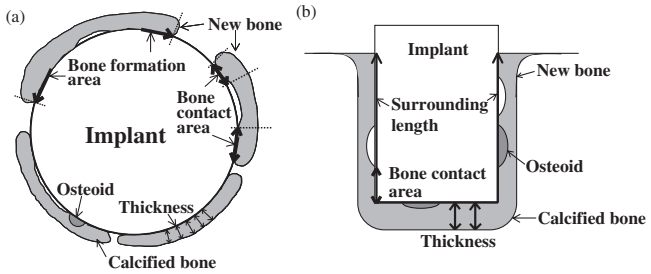

Fig. 4 Schematic illustration for estimating morphometrical parameters of new bone in transverse (a) and vertical (b) undecalcified bone sections.

(Quantimet 500+, Leica Co., Ltd.) and by the analysis of an optical micrograph using Mac Scope (Mitani Shoji). The means and standard deviations were calculated from the results obtained for the three to five rats (n = 3 to 5).

3. Experimental Results

3.1 Histological analysis

Figure 5 shows the optical micrograph of the new bone formed surrounding the Ti–15Zr–4Nb–4Ta alloy implant using the undecalcified bone sections stained with the toluidine blue and Villanueva stains at 12 weeks after implantation. The Ti–15Zr–4Nb–4Ta alloy implant was completely surrounded by the new bone in both the transverse (a) and vertical (b) sections. The new bones formed on the Co–Cr–Mo, Ti–6Al–4V and Ti–15Zr–4Nb–4Ta alloy implants stained using various stains are compared in Fig. 6. The new bones were well formed around all the alloy implants in the bone marrow. Neither the resorption of bone nor abnormalities such as the presence of foreign-body giant cells and infiltration of inflammatory cells were observed in all the alloy implants throughout the implantation period. In the new bone-metal interface, thin osteoid layers were observed in all the alloy implants. The osteoid layers around

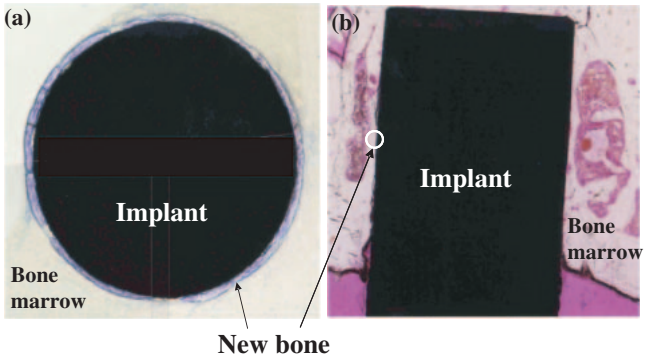

Fig. 5 Optical micrograph of new bone formed surrounding Ti–15Zr–4Nb–4Ta alloy implant at 12 weeks after implantation. (a) Transverse section of undecalcified bone stained using toluidine blue, (b) vertical section of undecalcified bone stained using Villanueva stain.

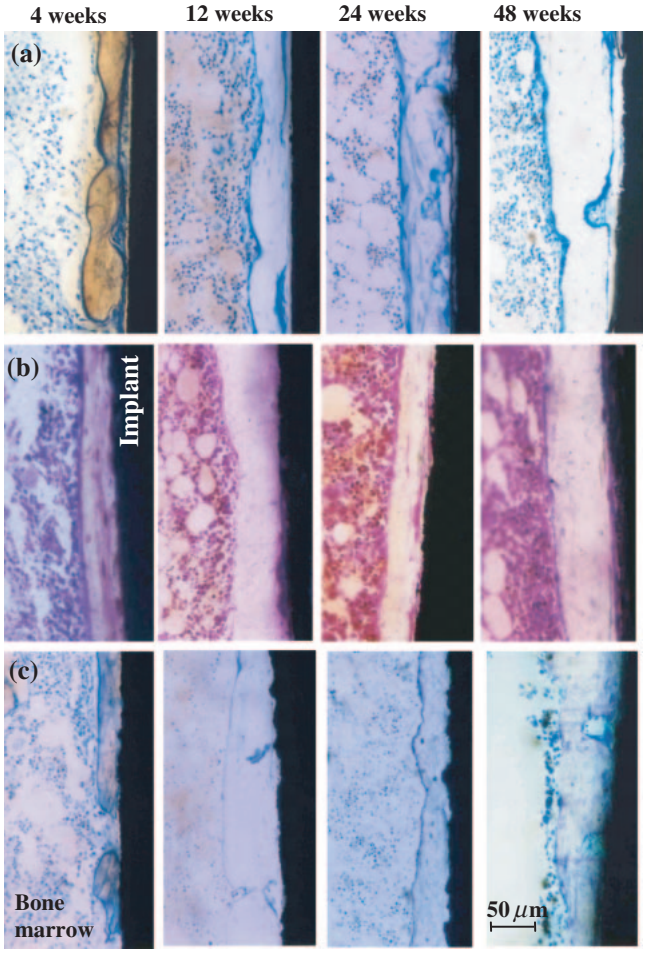

Fig. 6 Comparison of new bones formed on Co–Cr–Mo, Ti–6Al–4V and Ti–15Zr–4Nb–4Ta alloy implants (vertical undecalcified section). (a) Co–Cr–Mo alloy implant stained using Giemsa stain, (b) Ti–6Al–4V alloy implant stained using Villanueva stain (bright field), (c) Ti–15Zr–4Nb–4Ta alloy implant stained using toluidine blue stain.

the Co–Cr–Mo and Ti–15Zr–4Nb–4Ta alloy implants stained using the Villanueva stain are compared in Fig. 7. The osteoid layers formed around the Co–Cr–Mo alloy implants were slightly thicker than those formed around the Ti–6Al–4V and Ti–15Zr–4Nb–4Ta alloy implants. A tendency

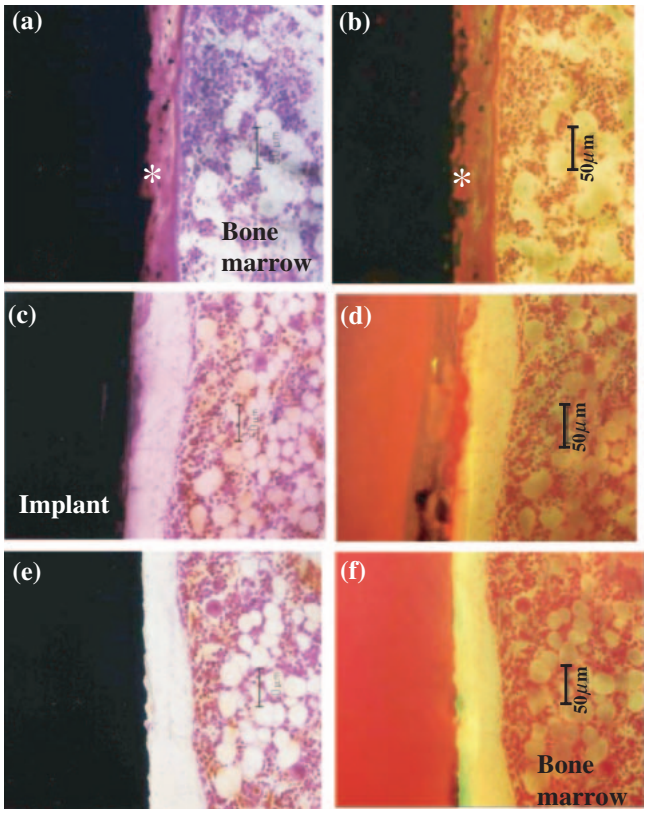

Fig. 7 Osteoid observed in new bone-Co–Cr–Mo alloy implant interface stained using Villanueva stain. (a), (c), (e) Bright field, (b), (d), (f) fluorescence, (a), (b) 4 weeks after implantation, and (c), (d), (e), (f) 12 weeks after implantation.

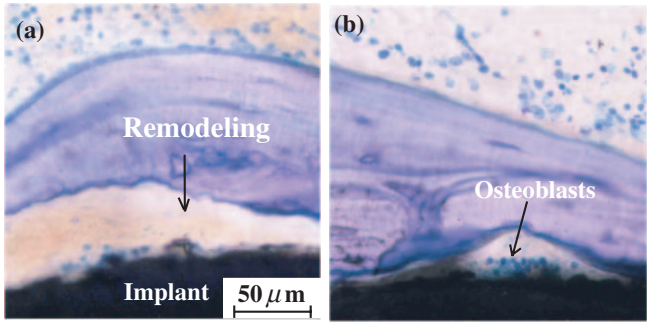

Fig. 8 Bone remodeling in new bone-implant interface in the transverse undecalcified sections stained using toluidine blue stain. (a) New bone-Co–Cr–Mo alloy interface at 6 weeks after implantation, (b) new bone-Ti–15Zr–4Nb–4Ta alloy interface at 12 weeks after implantation.

similar to that in the vertical section was observed in the transverse undecalcified sections with the 316L stainless steel, Co–Cr–Mo, Ti–6Al–4V and Ti–15Zr–4Nb–4Ta alloy implants. The bone remodeling around the new bone-metal implant interface observed in the transverse undecalcified sections is shown in Fig. 8. A normal bone remodeling was observed in the bone-metal interface, and osteoblasts capable of differentiating into a new bone tissue were lined on the implant side in the new bone-metal implant interface. The new bone formed around the metal implant developed into a calcified bone consisting of lamellar structure with increasing implantation period. Many osteocytes were observed in the lamellar bone tissue. The decalcified bone tissues stained using the AM and HE stains are shown in Figs. 9(b) to (e). A capsulated fibrous connective tissue was observed in the Co–Cr–Mo alloy section at 48 weeks after long-term implanta-

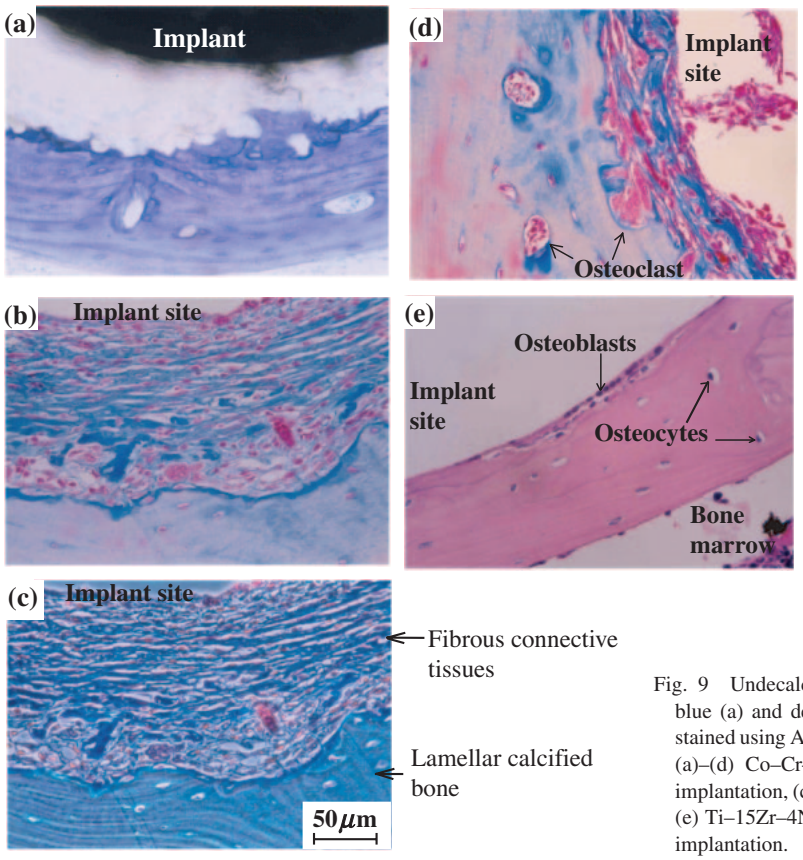

Fig. 9 Undecalcified stained using toluidine blue (a) and decalcified bone tissue [(b)–(e)] stained using AM [(b)–(d)] and HE [(e)] stains. (a)–(d) Co–Cr–Mo alloy at 48 weeks after implantation, (c) polarized optical micrograph, (e) Ti–15Zr–4Nb–4Ta alloy at 12 weeks after implantation.

tion, as shown in Figs. 9(a) to (d). This capsulated fibrous connective tissue was also observed in the 316L stainless steel section at 48 weeks after implantation. Many osteoclasts were observed at the interface between the fibrous connective tissue and lamellar bone tissue. Osteoblasts and osteocytes were observed in the decalcified bone section of the Ti–15Zr–4Nb–4Ta alloy implant stained using the HE stain at 12 weeks after implantation, as shown in Fig. 9(e).

3.2 Osteocompatibility

Osteocompatibilities obtained using the four morphometrical parameters for 316L stainless steel, Co–Cr–Mo, Ti–6Al–4V and Ti–15Zr–4Nb–4Ta alloy implants are compared in Figs. 10 to 13. The new bone formation rates in both the transverse and vertical sections were more than 90% in the early implantation period for all the alloy implants (Fig. 10). Thereafter, no marked changes were observed in any observation period. The bone contact rates in the vertical

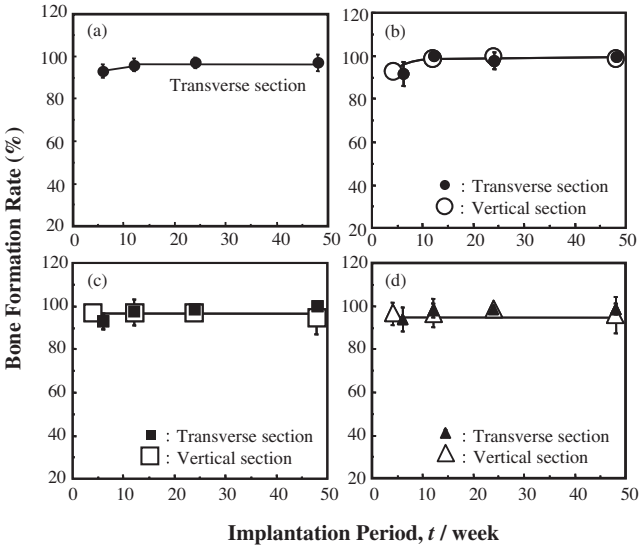

Fig. 10 Comparison of new bone formation rates for 316L stainless steel (a), Co–Cr–Mo (b), Ti–6Al–4V (c), and Ti–15Zr–4Nb–4Ta (a) alloy implants.

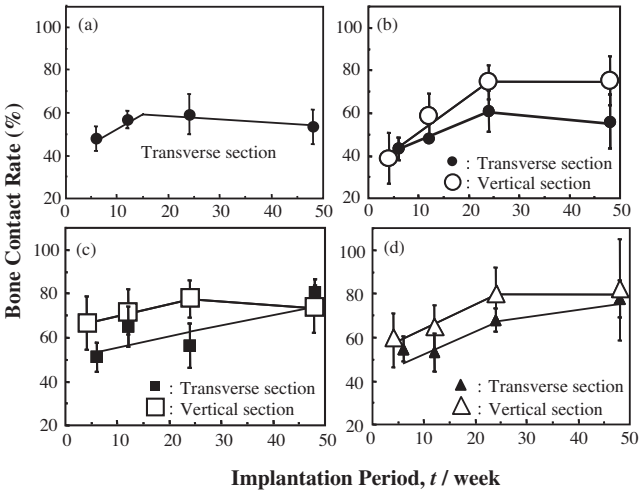

Fig. 11 Comparison of bone contact rates for 316L stainless steel (a), Co–Cr–Mo (b), Ti–6Al–4V (c), and Ti–15Zr–4Nb–4Ta (d) alloy implants.

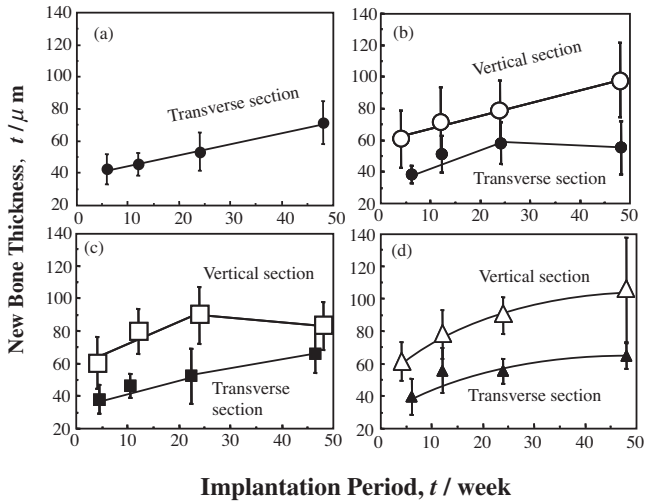

Fig. 12 Comparison of new bone thicknesses for 316L stainless steel (a), Co–Cr–Mo (b), Ti–6Al–4V (c), and Ti–15Zr–4Nb–4Ta (d) alloy implants.

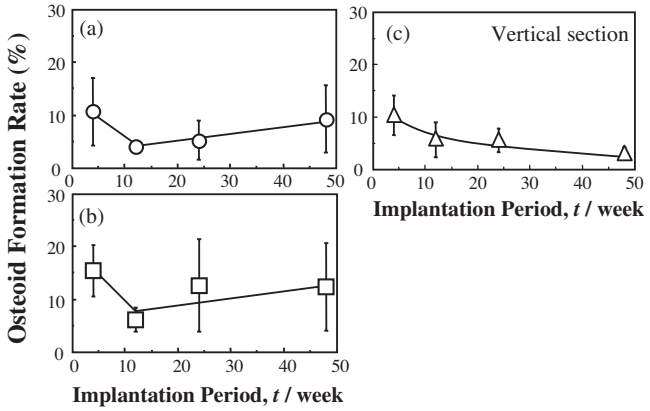

Fig. 13 Comparison of osteiod formation rates for Co–Cr–Mo (a), Ti–6Al–4V (b), and Ti–15Zr–4Nb–4Ta (c) alloy implants.

section tended to be higher than that in the transverse section (Fig. 11). The bone contact rates in the vertical sections of Co–Cr–Mo, Ti–6Al–4V and Ti–15Zr–4Nb–4Ta alloy implants at 4 weeks after implantation were 40 ± 12, 67 ± 12 and $59 \pm 12\%$, respectively. A significant difference in bone contact rate at 4 weeks after implantation was observed between the Co–Cr–Mo and two Ti alloy implants ($p < 0.05$). At 12 weeks after implantation, the values were 59 ± 11, 72 ± 10 and $64 \pm 11\%$, respectively. These values gradually increased to approximately more than 75% at 24 weeks after implantation, and thereafter, remained almost unchanged. Statistical analysis showed no significant difference in bone contact rate between the Ti–6Al–4V and Ti–15Zr–4Nb–4Ta alloy implants at $p = 0.05$. The thicknesses of the new bones formed around the alloy implants are compared in Fig. 12. The new bone thickness in the vertical section tended to be higher than that in the transverse section. The new bone thicknesses in the vertical sections of Co–Cr–Mo, Ti–6Al–4V and Ti–15Zr–4Nb–4Ta alloy implants were approximately 60 μm at 4 weeks after implantation. No difference in new bone thickness between the Ti–6Al–4V and Ti–15Zr–4Nb–4Ta alloy implants was observed. The osteoid

formation rates of the new bones formed around the alloy implants are compared in Fig. 13. The osteoid formation rates were approximately $11 \pm 6\%$ at 4 weeks after implantation in the Co–Cr–Mo alloy implant. In the Ti–15Zr–4Nb–4Ta alloy implant, the osteoid formation rates were 10 ± 4, 6 ± 3, 6 ± 2, and $3 \pm 1\%$ at 4, 12, 24 and 48 weeks after implantation, respectively. In contrast, in the Co–Cr–Mo and Ti–6Al–4V alloy implants, osteoid formation rates slightly increased from 24 up to 48 weeks after implantation, and the values were $9 \pm 6\%$ and $12 \pm 8\%$ at 48 weeks, respectively. Thus, the four morphometrical parameters obtained in rat implantation are valuable for the evaluation of osteocompatibility of biomaterials.

4. Discussion

For long-term implantation, the investigation of osteocompatibility of the metal implants is an important method. It was clarified that the four morphometrical parameters, namely, new bone formation rate, bone contact rate, new bone thickness and osteoid formation rate, were important for the evaluation of osteocompatibility of biomaterials. In view of animal protection in recent years, histological and morphometrical analyses using rats are important for the evaluation of osteocompatibility of biomaterials. The interface between the newly formed bone around the implant and metal implant is typically loose in the decalcifed bone section, when the metal implant is pushed out during the preparation. On the other hand, undecalcified bone sections, embedded in resin and cut including the metal, are advantageous in the determination of new bone-material interface.

AM staining is a typical method of stain selective staining of collagen fibers using aniline blue, one of the fibrous connective tissues. In the early stage of implantation, the osteoid was stained using aniline blue on the implant side of the new bone, and the calcified bone was stained in red on the outside. This tendency was consistent with that in the case of using TB, in which a new bone was stained light blue on the outside and deeply stained in the interface with the implant. The fibrous connective tissue was observed around the 316L stainless steel and Co–Cr–Mo alloy implants at 48 weeks after implantation. This result was consistent with the fact that the stainless steel and Co–Cr–Mo alloy have been classified in the group of metals encapsulated by the fibrous connective tissue (capsule type).[6] The bone contact rate of the Ti–6Al–4V alloy implant tended to be slightly lower than that of the Ti–15Zr–4Nb–4Ta alloy implant at 48 weeks after long-term implantation. The bone contact rate of the Ti–6Al–4V alloy implant is lower than that of the commercially pure Ti implant.[7,8]

Metals from orthopaedic implants are released by various mechanisms, including corrosion and mechanically accelerated electrochemical processes such as stress corrosion and corrosion fatigue.[9] The toxic effects of metals released from prosthetic implants have been reviewed.[10] Stainless steel and Co–Cr–Mo and Ti–6Al–4V alloys having cytotoxic elements, such as Co, Cr, Ni and V, have become a subject of discussion. To compare the release properties of various metal elements *in vivo*, trace quantities of metals accumulating in the bone tissue after implantation into the rat tibia for up to 48 weeks have been examined.[11] The Fe concentration in the bone tissue with the 316L stainless steel implant was relatively high, and it rapidly increased up to 12 weeks after implantation and then decreased thereafter. The Ni concentration in the bone tissue with the 316L stainless steel implant increased up to 6 weeks after implantation and then gradually decreased thereafter. On the other hand, the Co concentration in the tibia tissue with the Co–Cr–Mo alloy implant was low, and it increased up to 24 weeks and slightly decreased at 48 weeks after implantation. The Cr concentration tended to be higher than the Co concentration. This Cr concentration linearly increased up to 12 weeks and then decreased toward 48 weeks in the tibia tissues with the 316L stainless steel or Co–Cr–Mo alloy implant. Minute quantities of Ti, Al and V in the tibia tissues with the Ti–6Al–4V implant were observed. The Ti concentration in the tibia tissues with the Ti–15Zr–4Nb–4Ta implant was lower than that in the tibia tissues with the Ti–6Al–4V implant. The Zr, Nb and Ta concentrations were also very low. In the present study, the rate of direct bone contact with the two Ti alloys was significantly higher than that with the 316L stainless steel and Co–Cr–Mo alloy in the early stage of implantation. These findings are considered to reflect the *in vivo* results mentioned above.

It has been reported that of the 70 metals in the periodic table, only Zr and Ti support osteoblast growth and osteointegration.[12] Ti, Zr, Nb and Ta also have a considerably superior corrosion resistance. A new Ti alloy, Ti–15Zr–4Nb–4Ta alloy, without known cytotoxic metal elements such as V has been developed. The relative growth ratio of murine osteoblastic MC3T3-E1 cells is estimated using the following formula: (average number of cells per dish after 4 d incubation)/(average number of cells in the control). The relative growth ratio of the MC3T3-E1 (1.08 ± 0.02) cells with the Ti–15Zr–4Nb–4Ta alloy is slightly higher than that of MC3T3-E1 cells with the Ti–6Al–4V alloy (1.0).[13,14] In this study, the osteoid formation rate of the Ti–15Zr–4Nb–4Ta alloy implant slightly decreased with increasing implantation period, compared to those of Ti–6Al–4V and Co–Cr–Mo alloy implants. Metal releases of Co and Cr as major components of Co–Cr–Mo alloy, and V as the minor component of Ti–6Al–4V alloy might be responsible for the effects of these alloys on osteocompatibility.

Anodic polarization is enhanced when Zr, Nb, Ta or Pd is added because the resultant ZrO_2, Nb_2O_5, Ta_2O_5 and PdO strengthen the TiO_2 passive film that forms on Ti alloy.[15] The quantity of Ti released from the Ti–15Zr–4Nb–4Ta alloy is lower than that released from the Ti–6Al–4V alloy in simulated body fluids.[16] The quantity of (Zr+Nb+Ta) released is considerably lower than that of (Al+V) released. An acceptable level of biological response is expected when the Ti–15Zr–4Nb–4Ta alloy is used appropriately, because it consists of biocompatible elements and has excellent biocompatibility, corrosion resistance, microstructure, and mechanical and fatigue properties.[17–26] The facilities required for melting, forging and working of the Ti–15Zr–4Ta–4Nb alloy are the same as those required for such processes of the Ti–6Al–4V alloy. Bone plates, hip screws, intramedullary fixation and artificial hip joint implants are fabricated using

the same conventional manufacturing processes used for the Ti–6Al–4V alloy.[24] The increase in the incidence of allergy and the necessity for prolonged use require implants with a minimal metal release rate. Therefore, the Ti–15Zr–4Ta–4Nb alloy with a low metal release rate is considered advantageous for long-term surgical implantation.

5. Conclusions

Although thin osteoid layers in the new bone-metal implant interface were observed in all 316L stainless steel, Co–Cr–Mo, Ti–6Al–4V and Ti–15Zr–4Nb–4Ta alloy implants, the new bone was well formed around all the alloy implants in the bone marrow of the rat femur and tibia up to 48 weeks. Neither the resorption of bone nor inflammatory reactions such as that the presence of foreign-body giant cells and infiltration of inflammatory cells were evident in the histological examination of these implants. A normal bone remodeling was observed in the new bone-metal interface, and osteoblasts capable of differentiating into a new bone tissue were lined on the implant side in the new bone-metal implant interface. Many osteocytes were observed in the lamellar bone tissue. In the decalcified bone tissues stained using the Azan-Malloy stain, a capsulated fibrous connective tissue was observed in the 316L stainless steel and Co–Cr–Mo alloy implants at 48 weeks after long-term implantation. Many osteoclasts were observed at the interface between the fibrous connective tissue and lamellar bone tissue. The new bone formed around all the alloy implants developed into a calcified bone consisting of lamellar structure with increasing implantation period. The bone formation rates around all the alloy implants were markedly high, approximately more than 90% at 4 weeks after implantation, and thereafter, no remarkable change was observed. The bone contact rate and new bone thickness in the vertical section tended to be higher than those in the transverse section. In the early stage of implantation (4–12 weeks), the bone contact rate of Ti alloy implant was significantly higher than that of 316L stainless steel and Co–Cr–Mo alloy implants. In the late stage of implantation (24–48 weeks), the osteoid formation rates of Co–Cr–Mo and Ti–6Al–4V alloy implants tended to increase, but not significantly. Significant differences in the bone morphometrical parameters, suggesting osteocompatibility, were detected, although pathological findings were not evident. Histological examinations of undecalcified sections were essential for confirming the interface between the newly formed bone and the metal implant, and morphometrical parameters, namely, new bone formation rate, bone contact rate, new bone thickness and osteoid formation rate, suggested to be good markers of osteocompatibility for the investigation of various metal implants.

REFERENCES

1) G. L. Darimont, R. Cloots, E. Seidel and R. Lerrand: Biomaterials **23** (2002) 2569–2575.
2) Y. T. Sul, C. B. Johansson, K. Roser and T. Albrektsson: Biomaterials **23** (2002) 1809–1817.
3) C. J. Oosterbos, H. C. Vogely, M. W. Nijhof, A. Fleer, A. J. Verbout, A. J. Tonino and W. J. Dhert: J. Biomed. Mater. Res. **60** (2002) 339–347.
4) S. Vercaigne, J. G. Wolke, I. Naert and J. A. Jansen: Clin. Oral Implants Res. **11** (2000) 314–324.
5) C. J. Ivanoff, C. Hallgren, G. Widmark, L. Sennerby and A. Wennerberg: Clin. Oral Implants Res. **12** (2001) 128–134.
6) S. G. Steinemann: *Evaluation of Biomaterials*. eds. G. D. Winter, J. L. Leray and K. de Goot, (Wiley, Chichester, 1980) pp. 1–34.
7) C. B. Johansson, L. Sennerby and T. Albrektsson: Int. J. Oral Maxillofac Implant **6** (1991) 437–441.
8) C. B. Johansson, C. H. Han, A. Wennerberg and T. Albrektsson: Int. J. Oral Maxillofac Implant **13** (1991) 315–321.
9) J. J. Jacobs, C. Silverton, N. J. Hallab, A. K. Skipor, L. Patterson, J. Black and J. O. Galante: Clin. Orthop. Related Res. **358** (1999) 173–180.
10) K. L. Wapner: Clin. Orthop. Related Res. **271** (1991) 12–20.
11) Y. Okazaki, E. Gotoh, T. Manabe and K. Kobayashi: Biomaterials **25** (2004) 5913–5920.
12) S. G. Steinemann: *Materials for Medical Engineering*, eds. H. Stallforth and P. Revell, *Euromat 99*, Volume 2, (Wiley-VCH, Weinheim, 1999), pp. 199–203.
13) Y. Okazaki and Y. Ito: Adv. Eng. Mater. **2** (2002) 278–281.
14) Y. Okazaki: Curr. Opini. Solid State and Mater. Sci. **5** (2001) 45–53.
15) Y. Okazaki, T. Tateishi and Y. Ito: Mater. Trans., JIM **38** (1997) 78–84.
16) Y. Okazaki and E. Gotoh: Biomaterials **26** (2005) 11–21.
17) Y. Okazaki, Y. Ito, A. Ito and T. Tateishi: Mater. Trans., JIM **34** (1993) 1217–1222.
18) Y. Okazaki, A. Ito, T. Tateishi and Y. Ito: Mater. Trans., JIM **35** (1994) 58–66.
19) A. Ito, Y. Okazaki, T. Tateishi and Y. Ito: J. Biomed. Mater. Res. **29** (1995) 893–900.
20) Y. Okazaki, Y. Ito, A. Ito and T. Tateishi: *Medical Applications of Titanium and Its Alloys: The Material and Biological Issues*, ASTM STP 1272, eds. S. A. Brown and J. E. Lemons (ASTM 1996) pp. 45–59.
21) Y. Okazaki, S. Rao, T. Tateishi and Y. Ito: Mater. Sci. Eng. A **243** (1998) 250–256.
22) Y. Okazaki, S. Rao, Y. Ito and T. Tateishi: Biomaterials **19** (1998) 1197–1215.
23) Y. Okazaki and E. Nishimura: Mater. Trans., JIM **41** (2000) 1247–1255.
24) Y. Okazaki and E. Gotoh: Mater. Trans., JIM **43** (2002) 2943–2948.
25) Y. Okazaki and E. Gotoh: Mater. Trans., JIM **43** (2002) 2949–2955.
26) Y. Okazaki: Mater. Trans., JIM **43** (2002) 3134–3141.